39th IAHR WORLD CONGRESS
GRANADA, SPAIN 2022
From Snow to Sea
19-24 June 2022

Proceedings of the 39th IAHR World Congress
19-24 June 2022
Granada, Spain
DOI number

# Influence of a Rigid Cylinder on Flow Structure over a Backward-Facing Step

MILAD ABDOLLAHPOUR [1], PAOLA GUALTIERI [2], CARLO GUALTIERI [3]

[1, 2, 3] University of Napoli Federico II, Napoli, Italy
[1] m.abdolahpour@yahoo.com, [2] paola.gualtieri@unina.it, [3] carlo.gualtieri@unina.it

## Abstract

In the present study, laminar and turbulent flow over a backward-facing step (BFSF) where a cylinder was placed immediately downstream of the step was investigated through numerical simulation using OpenFOAM. In laminar flow mean errors between numerical and literature experimental data for velocity profiles and reattachment lengths were lower than 8.1% and 18%, respectively. The cylinder significantly modified the structure of recirculating flow over the BFSF. In addition, the cylinder increased the skewness of the velocity profiles, and the location of the maximum velocity shifted towards the upper wall. In turbulent flow, the results from several RANS models (standard k-ε, RNG k-ε, standard k-ω, SST k-ω, and RSM (SSG)) were compared with literature experimental data. The average error in predicting reattachment length and velocity profiles ranged from 2.2% to 28.5% and from 7.8% to 14.5%, respectively. The most accurate model in predicting reattachment length and velocity profiles was the standard k-ε and SST k-ω models respectively. The cylinder modified flow structure and the distribution of turbulent kinetic energy, whose largest value was found downstream of a cylinder in the separated shear layer.

**Keywords:** BFSF, cylinder, Numerical simulation, OpenFOAM

## 1. INTRODUCTION

The backward-facing step flow (BFSF) is a classical benchmark in Fluid Mechanics involving flow separation, reattachment, and vortex evolution (Chen et al. 2018). Hence, within the last decades, several experimental (Armaly et al., 1983; Lee and Mateescu, 1998; Bouda et al., 2008; Erturk, 2008; Tihon et al., 2012; Gautier and Aider, 2014; Chen et al., 2018; Wang et al., 2019; Bhatt et al., 2021), as well as numerical studies (Biswas et al., 2004; Gualtieri, 2005; Selimefendigil and Öztop., 2013; Jehad et al., 2015; Choi and Nguyen, 2016, and Moosavi et al., 2021), were carried out. Moreover, BFSF with new geometric designs have been studied in recent years, such as the wavy bottom design downstream of the step by Uruba et al. (2007), BFSF with cylinder by Kumar and Dhiman. (2012); Selimefendigil and Öztop. (2015); Park and Thornber. (2018), while some research was carried out on BFSF with an inclined step (Prihoda et al., 2012, Louda et al., 2013, Choi et al., 2016). These studies demonstrated that the reattachment length increases with increasing step angle, expansion ratio, and Reynolds number in laminar flow, while in turbulent flow such length is independent of the Reynolds number and increases with increasing step angle and expansion ratio.

However, few studies have addressed backward-facing step flow with a cylinder placed downstream of the step. The present study focused on the two-dimensional numerical simulation in both laminar and turbulent flow of that geometry to identify the effect of the cylinder on the general features of the BFSF, such as reattachment length, separation zones, and velocity profile. In turbulent flow, several turbulence models (standard k-ε, RNG k-ε, standard k-ω, SST k-ω, and RSM (SSG)) were comparatively analyzed. For all the numerical simulations, both in laminar and turbulent flow, the Open-Source Field Operation and Manipulation (OpenFOAM) software package was used.

## 2. MATERIAL AND METHODS

### 2.1 Computational Domain

Two geometries, BFSF 1 (without cylinder) and BFSF 2 (with cylinder) were created using the blockMesh dictionary, which creates fully structured hexahedral meshes. The design of the geometries was based on the experimental model of Armaly et al. (1983) (Figure 1). The expansion ratio ($ER=h_2/h_1$) was 2, which was very close to that of Armaly et al. (1983) ($ER$=1.94). In Figure 1, $h_1$ is the height of the inlet, $h_2$ is the height of the outlet and $h$ is the height of step. In BFSF 2, a cylinder with a diameter ($D$=4.5 mm) was added at 4.5 mm ($x/D$

=1) distance in the x-direction from the step edge. As shown in Figure 1, the top half of the cylinder was located above the top surface (mid-plane) of the step.

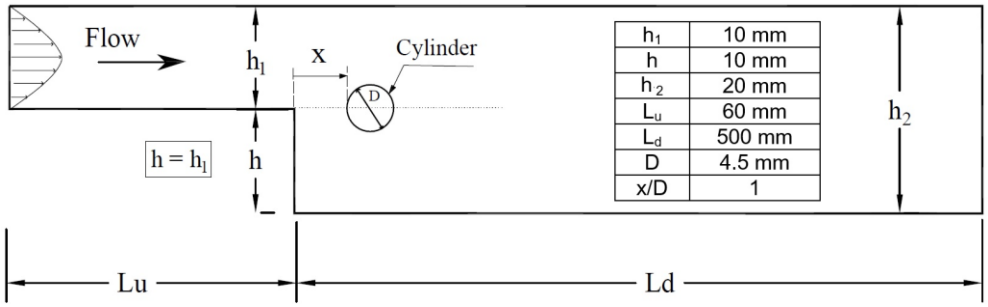


| | |
|---|---|
| $h_1$ | 10 mm |
| h | 10 mm |
| $h_2$ | 20 mm |
| $L_u$ | 60 mm |
| $L_d$ | 500 mm |
| D | 4.5 mm |
| x/D | 1 |

**Figure 1**. Sketch of the backward-facing step geometry with a cylinder

According to Armaly et al. (1983) the laminar regime occurs for Reynolds numbers based on the step height $Re_h < 900$, the transitional regime is in the range $900 < Re_h < 4950$ and the turbulent regime is $Re_h > 4950$. The present study was carried out in the Reynolds number range covering laminar and turbulent flows.

## 2.2 Laminar Flow

### *2.2.1 Numerical Method and Governing Equations*

The laminar flow was solved using icoFoam a transient solver of OpenFOAM. Continuity and momentum equations for two-dimensional flow in the laminar regime for an incompressible fluid can be written as:

Continuity equation

$$\frac{\partial u}{\partial x}+\frac{\partial v}{\partial y}=0 \quad [1]$$

Momentum equation

$$\rho\left(\frac{\partial u}{\partial t}+u\frac{\partial u}{\partial x}+v\frac{\partial u}{\partial y}\right)=-\frac{\partial p}{\partial x}+\rho g_x+\mu\left(\frac{\partial^2 u}{\partial x^2}+\frac{\partial^2 u}{\partial y^2}\right)$$

$$\rho\left(\frac{\partial v}{\partial t}+u\frac{\partial v}{\partial x}+v\frac{\partial v}{\partial y}\right)=-\frac{\partial p}{\partial y}+\rho g_y+\mu\left(\frac{\partial^2 v}{\partial x^2}+\frac{\partial^2 v}{\partial y^2}\right) \quad [2]$$

Where $\rho$ = fluid density; $\mu$ = dynamic viscosity; $p$ = pressure; $u$ and $v$ = velocity components in the x and y directions; and $g$ = acceleration of gravity.

### *2.2.2 Boundary and Initial Conditions*

The following boundary conditions were applied: A parabolic velocity profile was assigned to the inlet, zero gradient was assigned to the outlet, and fixedValue boundary was considered for cylinder, upper and lower walls. At the front and back, empty boundary condition was applied. Also, the initial values were defined for the problem. The tolerance of iterations was set to 1×10e-6. For the simulation, water with density $\rho$=997 Kg/m³ and dynamic viscosity ($\mu$) 8.905×10e-4 N.s/m² was selected as fluid. The Reynolds number based on the step height ($h$) was defined as $Re_h = \frac{Uh}{u}$ and the Reynolds number based on cylinder diameter ($D$) was calculated as $Re_c = \frac{UD}{u}$. Table 1 lists the values of Reynolds numbers in laminar flow.

**Table 1**. The range of Reynolds numbers based on the step height and cylinder diameter

| | | | | | | | | | |
|---|---|---|---|---|---|---|---|---|---|
| **$Re_h$ (Based on step height)** | 75 | 112 | 158 | 219 | 336 | 420 | 544 | 672 | 755 |
| **$Re_c$ (Based on cylinder diameter)** | 34 | 50 | 71 | 99 | 151 | 189 | 245 | 302 | 340 |

## 2.3 Turbulent Flow

### *2.3.1 Numerical Method and Governing Equations*

A transient solver, pisoFoam was used for the turbulent flow. Thus, for the two-dimensional steady flow of an incompressible fluid, Reynolds averaged Navier-Stokes equations for continuity and momentum are given by:

Continuity equation

$$\frac{\partial \bar{u}}{\partial x}+\frac{\partial \bar{v}}{\partial y}=0 \quad [3]$$

Momentum equation

$$\frac{\partial \bar{u}}{\partial t}+\bar{u}\frac{\partial \bar{u}}{\partial x}+\bar{v}\frac{\partial \bar{u}}{\partial y}=\ g_x-\frac{\partial \bar{p}}{\partial x}+\upsilon\nabla^2\bar{u}+\frac{\partial}{\partial x}(\upsilon_t\frac{\partial \bar{u}}{\partial x})+\frac{\partial}{\partial y}(\upsilon_t\frac{\partial \bar{u}}{\partial y})$$
$$\frac{\partial \bar{v}}{\partial t}+\bar{u}\frac{\partial \bar{v}}{\partial x}+\bar{v}\frac{\partial \bar{v}}{\partial y}=\ g_y-\frac{\partial \bar{p}}{\partial y}+\upsilon\nabla^2\bar{v}+\frac{\partial}{\partial x}(\upsilon_t\frac{\partial \bar{v}}{\partial x})+\frac{\partial}{\partial y}(\upsilon_t\frac{\partial \bar{v}}{\partial y}) \quad [4]$$

Where $\upsilon$ = kinematic viscosity; and $\upsilon_t$ = turbulent eddy kinematic viscosity. Several turbulence models, such as standard k-ε, RNG k-ε, standard k-ω, SST k-ω, and RSM (SSG) turbulence models, were comparatively used. The standard k-ε is the most widely applied model in turbulence modeling. Its formulation is presented in equations 5 - 7:

$$\frac{\partial k}{\partial t}+\bar{u}_j\frac{\partial k}{\partial x_j}=\frac{\partial}{\partial x_j}[(\upsilon+\frac{\upsilon_t}{\sigma_k})\frac{\partial k}{\partial x_j}]\ -\ \upsilon_t\frac{\partial \bar{u}_i}{\partial x_j}(\frac{\partial \bar{u}_i}{\partial x_j}+\frac{\partial \bar{u}_j}{\partial x_i})-\varepsilon \quad [5]$$
$$\frac{\partial \varepsilon}{\partial t}+\bar{u}_j\frac{\partial \varepsilon}{\partial x_j}-\frac{\partial}{\partial x_j}[(\upsilon+\frac{\upsilon_t}{\sigma_\varepsilon})\frac{\partial \varepsilon}{\partial x_j}]=\ C_1\frac{\varepsilon}{k}\upsilon_t\frac{\partial \bar{u}_i}{\partial x_j}(\frac{\partial \bar{u}_i}{\partial x_j}+\frac{\partial \bar{u}_j}{\partial x_i})-C_2\frac{\varepsilon^2}{k} \quad [6]$$
$$\upsilon_t=\rho C_\mu\frac{k}{\varepsilon} \quad [7]$$

Where $u_i$ = velocity component; $k$ = turbulent kinetic energy; $\varepsilon$ = turbulent kinetic energy dissipation rate. The rest of terms ($C_1$, $C_2$, $C_\mu$, $\sigma_k$, $\sigma_\varepsilon$) are model parameters that, in the standard k-ε model, are 1.44, 1.92, 1.3, 1, and 1.3, respectively. At the inlet, the turbulent kinetic energy and dissipation rate can be estimated by:

$$k\ =\ \frac{3}{2}\ (|u_{reff}|T_i)^2 \quad [8]$$
$$\varepsilon=\frac{0.09^{0.75}k^{1.5}}{l} \quad [9]$$

Where $u_{reff}$ = inlet flow velocity (m/s); $l$ = 0.07$L$ ($L$ = characteristic inlet scale (m)); $T_i$ =turbulent intensity (5%). In omega-based models, $\omega$ is the specific dissipation rate, which is estimated as:

$$\omega\ =\ \frac{k^{0.5}}{0.09^{0.25}l} \quad [10]$$

### *2.3.2 Boundary and Initial Conditions*

Boundary conditions and initial values are listed in Table 2. The Reynolds number based on the step height was $Re_h$=9000, which was equal to $Re_c$=4050 based on cylinder diameter.

**Table 2.** Boundary conditions and the input value of backward-facing step in turbulent flow

| Boundary type description | | inlet | outlet | Wall (upper wall, lower wall, cylinder) | Input values |
|---|---|---|---|---|---|
| **Pressure** | **p (kg /s.m2)** | zeroGradient | fixedValue | zeroGradient | 0 |
| **Velocity** | **u (m/s)** | fixedValue | inletOutlet | noSlip | 0.801 |
| **Turbulence fields** | **k ($m^2/s^2$)** | fixedValue | zeroGradient | kqRWallFunction | 0.002406 |
| | **ε ($m^2/s^3$)** | fixedValue | zeroGradient | epsilonWallFunction | 0.0277 |
| | **ω (1/s)** | fixedValue | zeroGradient | omegaWallFunction | 124.82 |

## 3. RESULTS AND DISCUSSION

### 3.1 Laminar Flow

### *2.3.3 Reattachment Length*

The most important characteristics in BFSF are flow separation and reattachment. The adverse pressure gradient due to the sudden expansion at the edge of the step induced this separated flow. A sketch of flow over the backward-facing step with and without cylinder is shown in Figure 2.

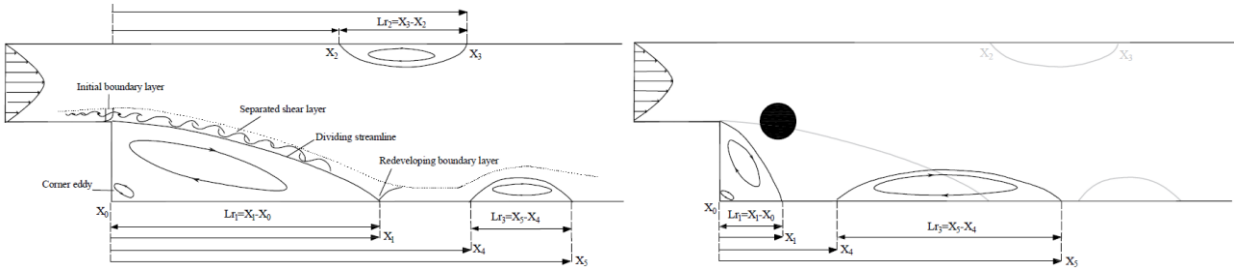


(a) (b)

**Figure 2**. Sketch of the flow a) BFSF 1 b) BFSF 2 (modified from Erturk, 2008)

In the classical BFSF (BFSF 1), flow pattern involves several different flow regions: initial boundary layer, separated free shear layer, corner eddy, primary recirculation zone on the lower wall ($Lr_1$), second recirculation zone on upper wall ($Lr_2$), redeveloping boundary layer, and third recirculation zone on the lower wall ($Lr_3$), as shown in Figure 2-a. The physics of separation regions could be described as follows: flow separated at the step ($X_0$) and reattached to the lower wall ($X_1$) which is called primary recirculation zone having a length $Lr_1$ which increased as $Re_h$. In addition to the primary recirculation zone ($Lr_1$), a second recirculation zone ($Lr_2$) near the upper wall for $Re_h$ > 300 was reported in previous studies. Point $X_2$ shows the starting location of the recirculation zone and point $X_3$ is the corresponding end of this region on the upper wall. According to Erturk (2008), with an expansion ratio of 2 for $Re_h$ > 1275, a third recirculating zone was observed between points $X_4$ and $X_5$ with length $Lr_3$. Its length $Lr_3$ increased as $Re_h$ increased. However, Armaly et al. (1983) found that the third recirculation region ($Lr_3$) was in the early part of the transitional flow, and it was not observed for $Re_h$ > 1725. Cherdron et al. (1978) and Sparrow and Kaljes (1977) suggested that the third recirculation zone was caused by vortex shedding from the edge of the step. These vortices were thought to approach the wall, and the third recirculation zone might be due to the sharp change of flow direction that eddies experience (Armaly et al. 1983).

In the BFSF with a cylinder (BFSF 2), the flow separated at the step, but the dividing streamline was deviated by the cylinder to the lower wall and the reattachment point $X_1$ was found to be upstream than for BFSF 1. In addition, the second recirculation zone on the upper wall was missing, while the third recirculation zone was observed even at 75 <$Re_h$ ≤ 755, and it was placed upstream than in the BFSF 1. For BFSF 2, $Lr_1$ and $Lr_3$ increased as $Re_h$ increased. Figure 3 compares the normalized location of $X_5$ point between BFSF 2 of the present study and the numerical results of Erturk (2008) for a classical BFSF.

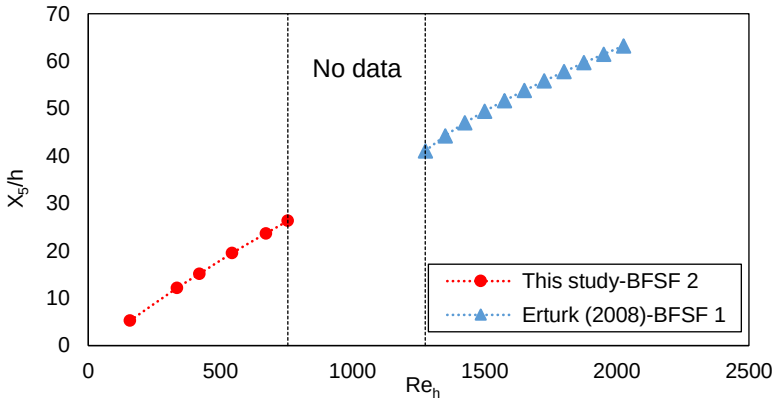


**Figure 3.** Dimensionless reattachment point of third recirculation region ($X_5/h$) vs. $Re_h$

Table 3 lists the value of normalized location of starting and ending recirculation zones in BFSF 1 and BFSF 2. In BFSF 2, while $X_4$ was unchanged $X_5$ as the $X_5/h$ increased as $Re_h$ increased.

**Table 3**. The reattachment and separation points of the recirculation zones vs. $Re_h$ in laminar flow

| | $X_1/h$ | | $X_2/h$ | | $X_3/h$ | | $X_4/h$ | | $X_5/h$ | |
|---|---|---|---|---|---|---|---|---|---|---|
| **$Re_h$** | BFSF1 | BFSF2 | BFSF1 | BFSF2 | BFSF1 | BFSF2 | BFSF1 | BFSF2 | BFSF1 | BFSF2 |
| **75** | 2.88 | - | - | - | - | - | - | - | - | - |
| **158** | 5.25 | 0.45 | - | - | - | - | - | 4.4 | - | 5.26 |
| **336** | 9.15 | 0.7 | 7.8 | - | 10.65 | - | - | 2.3 | - | 12.15 |
| **420** | 10.4 | 0.8 | 8.65 | - | 14.15 | - | - | 2.25 | - | 15.1 |
| **544** | 11.5 | 0.85 | 8.9 | - | 18.6 | - | - | 2.1 | - | 19.5 |
| **672** | 12.65 | 0.9 | 10.2 | - | 21.5 | - | - | 2.1 | - | 23.65 |
| **755** | 13.37 | 0.9 | 10.62 | - | 23.1 | - | - | 2.05 | - | 26.3 |

Figure 4 compares the primary recirculation zone ($Lr_1$) with experimental data of Armaly et al. (1983); Lee and Mateescu. (1998) and Tihon et al. (2010) as well as numerical studies of Gualtieri (2005) and Erturk (2008).

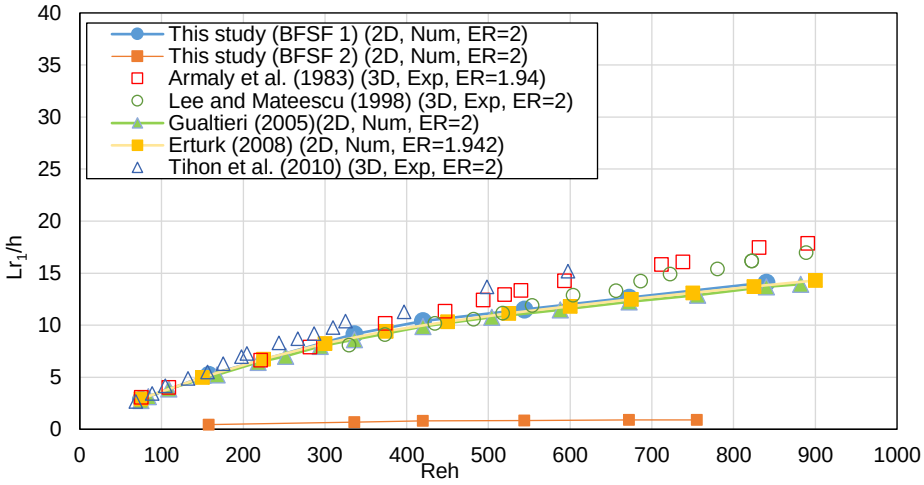


**Figure 4.** Dimensionless primary reattachment length $Lr_1$/h vs. $Re_h$ in laminar flow

The mean error between the present numerical results and literature numerical and experimental data was lower than 18% and 5 % respectively. The cylinder pushed the primary recirculation region upstream to the corner of the step and, hence, at each $Re_h$, $Lr_1$ was generally lower than that of BFSF 1.

### *2.3.4 Velocity Profiles*

The distribution of the u-velocity in BFSF 1 and BFSF 2 at $Re_h$=336 is shown in Figure 5. The cylinder partly deviated the flow to the lower wall.

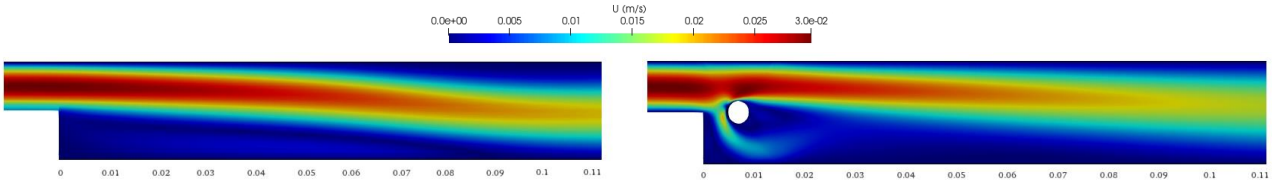


(a) (b)

**Figure 5**. Distribution of u-velocity at $Re_h$=336 a) BFSF 1 b) BFSF 2

The u-velocity profiles of BFSF 1 and BFSF 2 at $Re_c$ =34 and 302 are shown in Figures 6 and 7, The velocity profiles were consistent with the experimental data of Armaly et al. (1983) and numerical results of Gualtieri (2005). The mean error between numerical and literature data was lower than 8.1%.

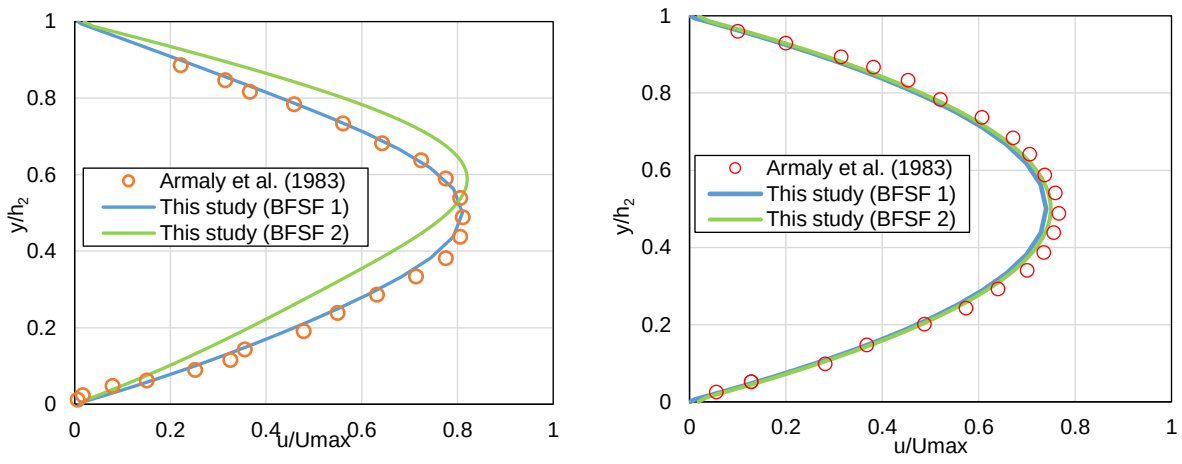


(a) (b)

**Figure 6.** Dimensionless u-velocity profiles ($u/U_{max}$) at $Re_c$=34 a) $x/h$=4.8 b) $x/h$=12.04

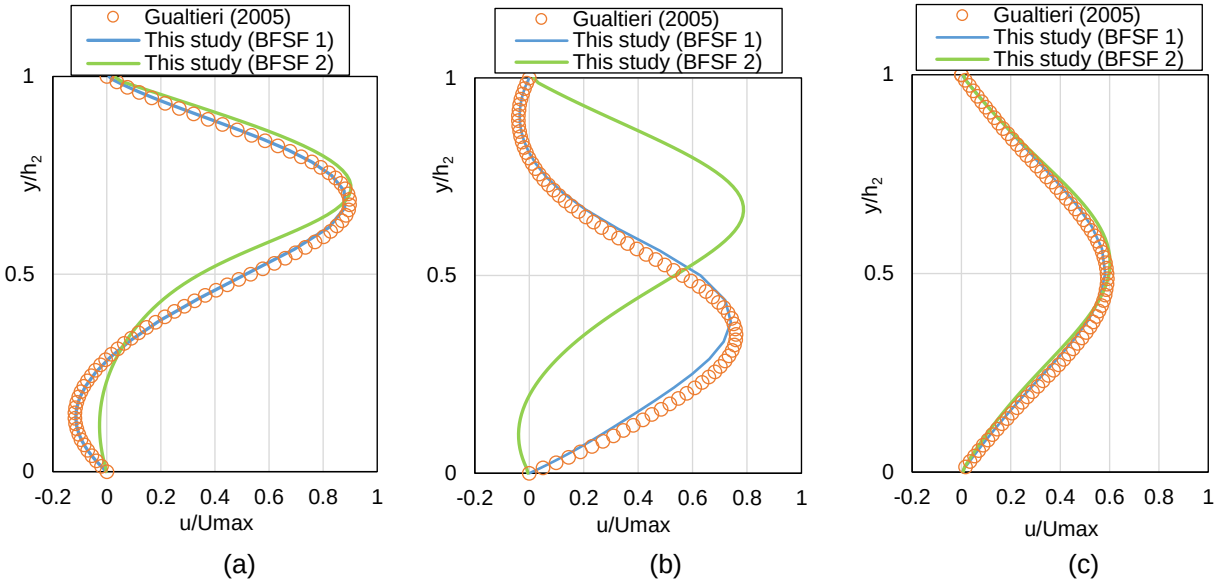


**Figure 7.** Dimensionless u-velocity profiles ($u/U_{max}$) at $Re_c$=302 a) $x/h$=7.5 b) $x/h$=15 c) $x/h$=30

In BFSF 2, with the incident flow toward the cylinder, the regular patterns of the vortex were shed rear of the cylinder. The maximum velocity values in BFSF 2 were a bit higher than in BFSF 1 and the location of the maximum velocities shifted towards the upper wall. But, more importantly, the cylinder increased the skewness of the velocity profiles. The skewness of velocity profiles were calculated for both BFSF 1 and BFSF 2 in the following locations: $x/h$ = 0.25 where the primary recirculation occurred and the velocity distribution was high; $x/h$ = 4.5, $x/h$ = 9 where was downstream of the cylinder and at $x/h$ = 28 the flow developed and reached the outlet of the geometry. In BFSF 2, the percentage of increasing skewness were 155, 190, 107 and 20 % at $x/h$ = 0.25, $x/h$ = 4.5, $x/h$ = 9 and $x/h$ = 28 respectively. The results indicated that the skewness of the velocity profile near the cylinder was larger than in other locations.

## 3.2 Turbulent Flow

### *3.2.1 Reattachment Length*

The reattachment length in BFSF 1 and BFSF 2 from standard k-ε, RNG k-ε, standard k-ω, SST k-ω, and RSM (SSG) was compared with literature experimental data and numerical results. The data were plotted in Figure 8 as the normalized reattachment length by the step height against Reynolds number $Re_h$.

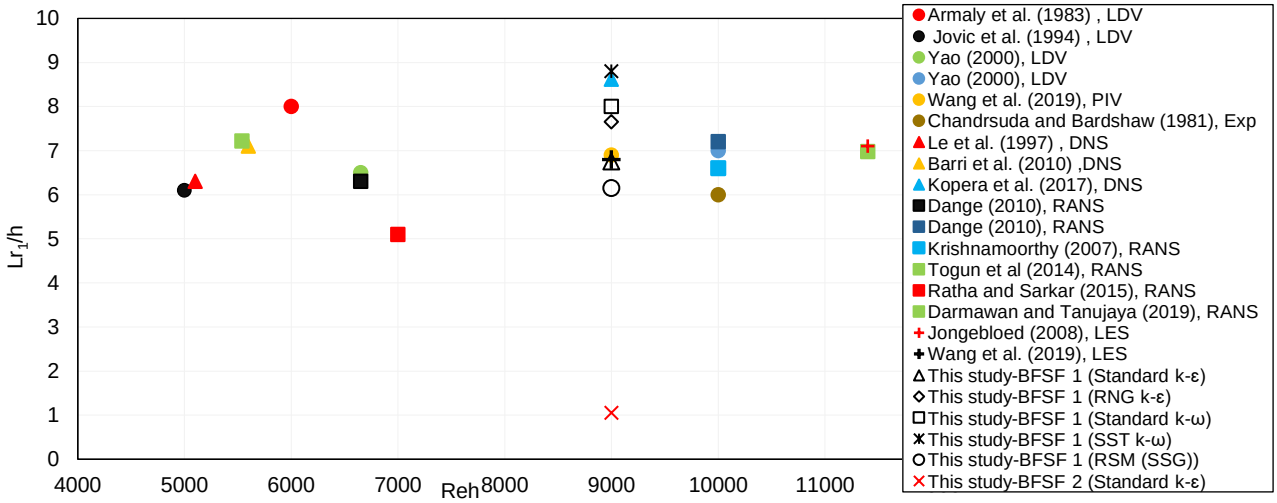


**Figure 8.** Dimensionless primary reattachment length ($Lr_1$/h) vs. $Re_h$ in turbulent flow

Most of the reattachment lengths of classical BFSF reported in the literature were between 5 and 8 times the step height. The present numerical results were compared with the PIV data of Wang et al. (2019) and the DNS results of Kopera et al. (2017). The mean error between the present numerical results and experimental data (PIV) of Wang et al. (2019) and the DNS results of Kopera et al. (2017) ranged from 2.2% to 27.5% and

2.3% to 28.5%, respectively. If compared with PIV measurements, the most accurate model in predicting reattachment length was the standard k-ε, followed by RNG k-ε, RSM (SSG), standard k-ω, and SST k-ω. Considering the accuracy and the calculation time of the models, only the standard k-ε model was used for BFSF 2. Table 4 lists the value of normalized location of reattachment lengths ($X_1/h$, $X_4/h$, and $X_5/h$) in BFSF 1 and BFSF 2.

**Table 4.** Dimensionless reattachment points of primary and third reattachment length in turbulent flow

| Case | Method | $X_1/h$ | $X_4/h$ | $X_5/h$ |
|---|---|---|---|---|
| **BFSF 1** | standard k-ε | 6.75 | - | - |
| | RNG k-ε | 7.65 | - | - |
| | standard k-ω | 8 | - | - |
| | SST k-ω | 8.8 | - | - |
| | RSM (SSG) | 6.15 | - | - |
| **BFSF 2** | standard k-ε | 1.05 | 6.51 | 7.2 |

As in laminar flow, the cylinder decreased $Lr_1$. In BFSF 2, a small third recirculation region ($Lr_3$) was observed far away from the primary recirculation zone on the lower wall. As previously pointed out, Armaly et al. (1983) reported third recirculation zone was not found in their study for $Re_h > 1725$. However, in the present study for BFSF 2, the third recirculation zone was observed even for $Re_h$ =9000. It is noted that the size of the third recirculation zone ($Lr_3$) was smaller than that of the primary recirculation zone ($Lr_1$).

### *3.2.2 Velocity Profiles*

As shown in Figure 9, the u-velocity profiles in BFSF 1 were compared with the results of Wang et al. (2019) and Kopera et al. (2017) in $x/Lr_1$ = 0.06, $x/Lr_1$ = 0.46, and $x/Lr_1$ = 0.93. Also, the velocity profiles of BFSF 2 were added to these plots. Note that in BFSF 2, the locations were scaled using $Lr_1$ from the standard k-ε model in BFSF 1, rather than that in BFSF 2.

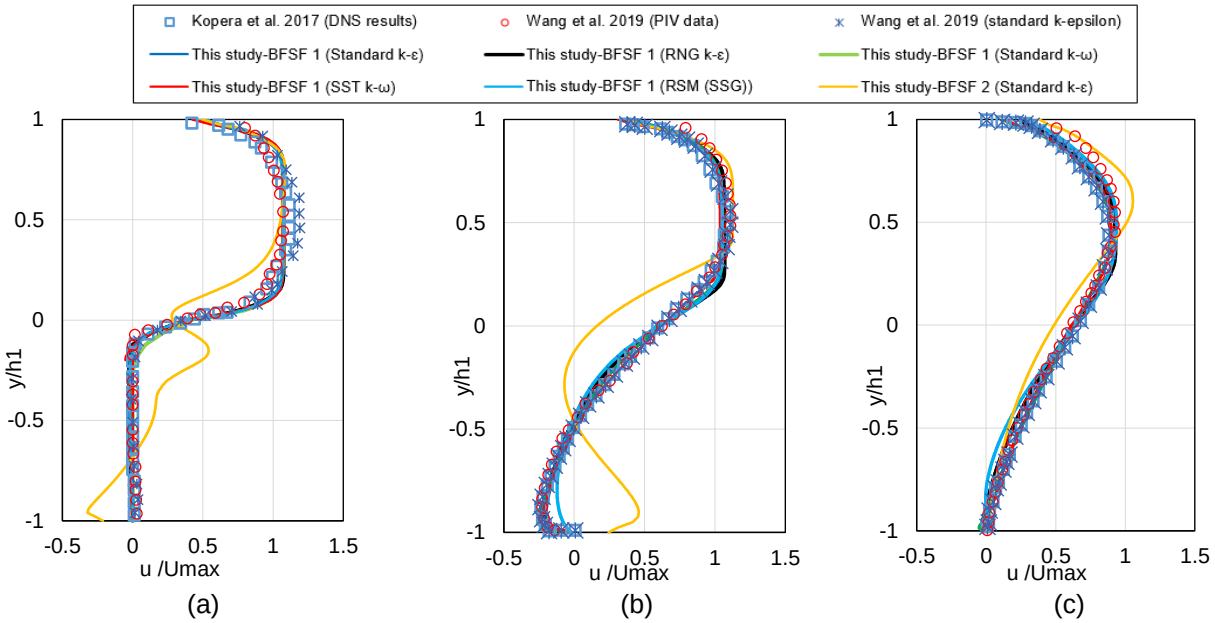


**Figure 9.** Dimensionless u-velocity profiles of BFSF 1 and BFSF 2 a) $x/Lr_1$=0.06 b) $x/Lr_1$=0.46 c) $x/Lr_1$=0.93

The first location ($x/Lr_1$ = 0.06) was placed just downstream of the step and it can be seen that the fully developed flow extended in all turbulence models. In $x/Lr_1$ = 0.46, where the primary recirculation occurred in BFSF 1, negative velocity was found near the lower wall, consistently with the DNS results by Kopera et al. (2017) and PIV data by Wang et al. ( 2019). In BFSF 1, the negative velocity in location $x/Lr_1$ = 0.46, represented the presence of inverse flow in the primary recirculation zone. The velocity near the lower wall for the RSM (SSG) model was smaller than the values obtained by the other models. However, in BFSF 2, positive velocity was found because this location ($x/Lr_1$ = 0.46) was placed between two recirculation zones ($Lr_1$ *and* $Lr_3$). In $x/Lr_1$ = 0.93, the standard k-ω, SST k-ω, and RNG k-ε models presented negative velocity because their $Lr_1$ was the largest among all models. The RSM (SSG) and standard k-ε models presented the highest velocity in the region near the lower wall. Far away from the cylinder ($x/Lr_1$ = 0.93) flow in both BFSF 1 and BFSF 2 had similar behavior in terms of separation and velocity profiles. As in laminar flow, in BFSF 2, the location of the maximum

velocity shifted towards the upper wall. As shown in Table 5, the average error between the present numerical results and literature experimental data was from 8.8 % to 12.3% and from 7.8 % to 14.5% if compared with the DNS results. The most accurate model in predicting velocity profiles was the SST k-ω, followed by the standard k-ω, RNG k-ε, the standard k-ε and RSM (SSG). The SST k-ω model was already recommended for cases with adverse pressure gradient and flow separation because it addresses the advantages of standard k-ω and standard k-ε models (Araujo and Rezende, 2017).

**Table 5**. The mean error (%) between numerical results with literature experimental and numerical results

| | Turbulence models | | | | |
|---|---|---|---|---|---|
| | **standard k-ε** | **RNG k-ε** | **standard k-ω** | **SST k-ω** | **RSM (SSG)** |
| **PIV data by Wang et al. (2019)** | 10.13 | 10.05 | 9.31 | 8.83 | 12.28 |
| **DNS results by Kopera et al. (2017)** | 10.6 | 10.56 | 8.43 | 7.82 | 14.43 |

*3.2.3 Turbulent kinetic energy (TKE)*

Figure 10 shows the distribution of turbulent kinetic energy of BFSF 1 and BFSF 2 for different turbulence models.

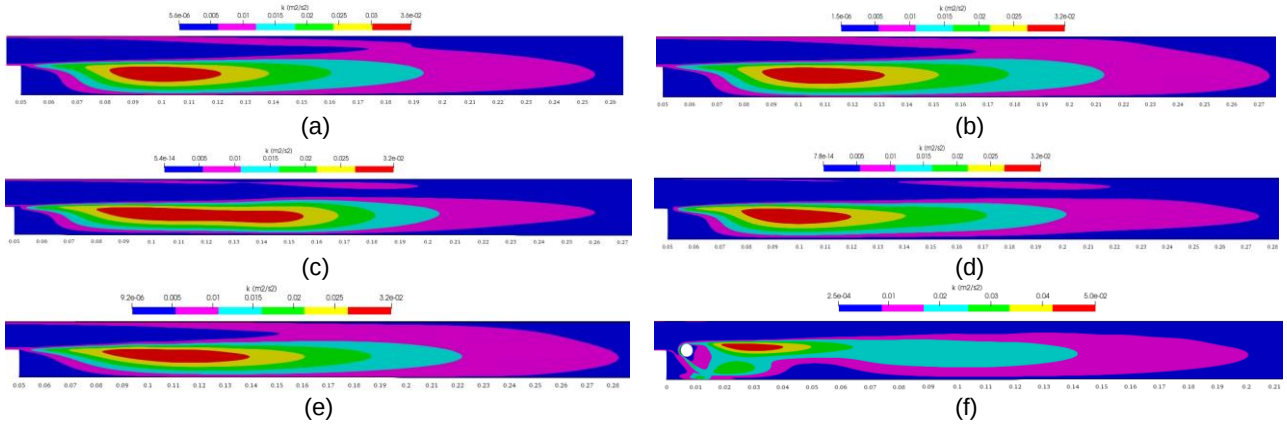


**Figure 10.** The distribution of turbulent kinetic energy a) BFSF 1 - Standard k-ε b) BFSF 1 - RNG k-ε c) BFSF 1 - Standard k-ω d) BFSF 1 - SST k-ω e) BFSF 1 - RSM (SSG) f) BFSF 2 - Standard k-ε

The distribution pattern was quite similar for all models. However, the cylinder changed the distribution of turbulent kinetic energy. In the BFSF 1, the TKE decreased monotonically starting from the step edge in the x-direction. Figure 11 shows vertical profiles of the turbulent kinetic energy normalized by maximum velocity value in *x/h*=0.02, *x/h*=0.05, and *x/h*=0.1.

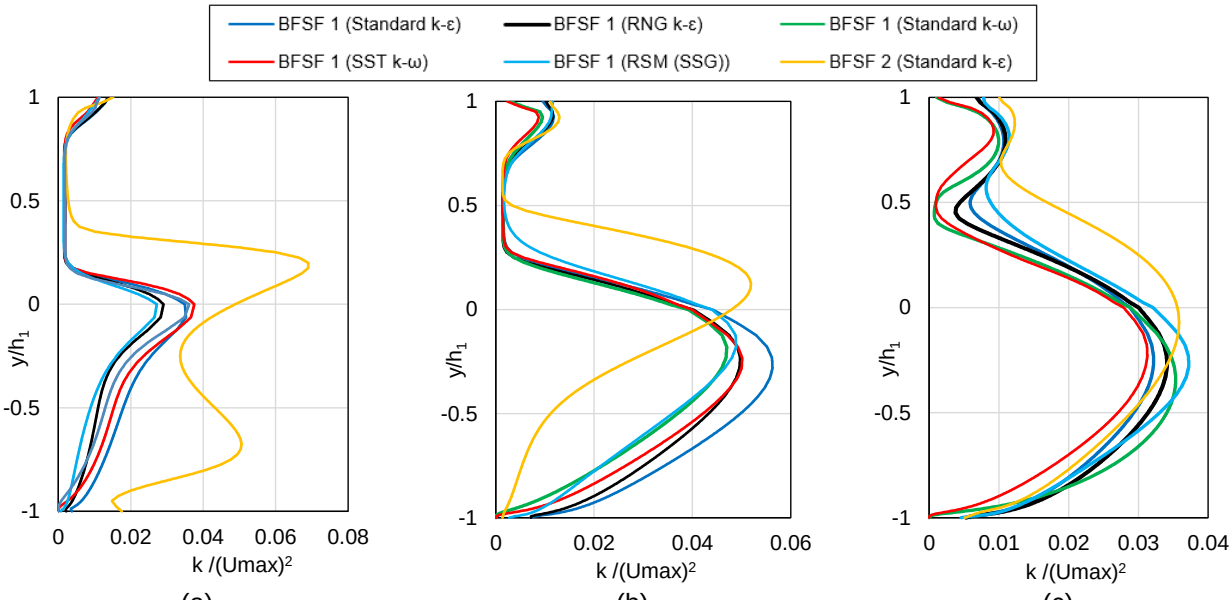


**Figure 11.** Dimensionless turbulence kinetic energy of BFSF 1 and BFSF 2 a) *x/h*=0.02 b) *x/h*=0.05 c) *x/h*=0.1

The maximum turbulent kinetic energy was below the mid-plane of step in regions of high shear flow. In BFSF 1, a sharp value of TKE ranged from $0.45 \leq x/Lr_1 \leq 1.45$. This result demonstrated that the peak value of TKE was approximately around the recirculation region and all turbulence models had similar amplitudes. However, in BFSF 2, the sharp value of TKE ranged from $1.9 \leq x/Lr_1 \leq 6.9$. The TKE value increased immediately downstream of the cylinder.

## 4. CONCLUSIONS

In the present study, two geometries were comparatively considered, namely the classical BFSF (BFSF 1) and a BFSF with a cylinder placed downstream of the step edge (BFSF 2), in both laminar and turbulent flow to identify how the cylinder affects flow structure. First, the numerical results for BFSF 1 were found to be in good agreement with the literature experimental and numerical results. The following conclusions can be summarized:

- In BFSF 1, three recirculation zone were observed: primary recirculation zone on the lower wall in laminar and turbulent regime; second recirculation zone at the upper wall for $Re_h>300$; and third recirculation zone on the lower wall in the early part of the transitional regime. In both laminar and turbulent flow, the cylinder pushed the primary recirculation region upstream to the corner of the step and its length decreased, while the second recirculation zone near the upper wall was missing in laminar flow. In BFSF 2 the third recirculation zone was observed even for laminar and turbulent flow and its location was placed upstream than in BFSF 1.
- The cylinder increased the skewness of the velocity profiles, and the location of the maximum velocity shifted towards the upper wall in the laminar and turbulent flow.
- In the BFSF 1, the standard k-ε model predicted the reattachment length better than the turbulence models which were used in this study. The RNG k-ε, standard k-ω, and SST k-ω models tended to overestimate the recirculation length and RSM (SSG) had a significantly short reattachment length as compared with literature PIV data. However, SST k-ω was the most accurate model in predicting velocity profiles.
- In the BFSF 1, the maximum turbulent kinetic energy was located downstream of the step, below the mid-plane of the step. However, in BFSF 2, the cylinder increased the turbulent kinetic energy and the location of the maximum TKE shifted towards the centerline of the channel.

## 5. REFERENCES

Araujo, P.P., and Rezende, A.L.T. (2017). Comparison of turbulence models in the flow over a backward-facing step. *International Journal of Engineering Research and Science*, *3*(11), 88-93.

Armaly, B.F., Durst, F., Pereira, J.C.F., and Schönung, B. (1983). Experimental and theoretical investigation of backward-facing step flow. *Journal of Fluid Mechanics*, 127, 473-496.

Barri, M., El Khoury, G.K., Andersson, H.I., and Pettersen, B. (2010). DNS of backward-facing step flow with fully turbulent inflow. *International Journal for Numerical Methods in Fluids*, 64(7), 777-792.

Bhatt, A., Ganesh, H., and Ceccio, S.L. (2021). Cavitating flow behind a backward facing step. *International Journal of Multiphase Flow*, 139, 103584.

Biswas, G., Breuer, M., and Durst, F. (2004). Backward-facing step flows for various expansion ratios at low and moderate Reynolds numbers. *Journal of Fluids Engineering*. 126(3), 362-374.

Bouda, N.N., Schiestel, R., Amielh, M., Rey, C., and Benabid, T. (2008). Experimental approach and numerical prediction of a turbulent wall jet over a backward facing step. *International Journal of Heat and Fluid Flow*, 29(4), 927-944.

Chandrsuda, C., and Bradshaw, P. (1981). Turbulence structure of a reattaching mixing layer. *Journal of Fluid Mechanics*, 110, 171-194.

Chen, L., Asai, K., Nonomura, T., Xi, G., and Liu, T. (2018). A review of Backward-Facing Step (BFS) flow mechanisms, heat transfer and control. *Thermal Science and Engineering Progress*, 6, 194-216.

Cherdron, W., Durst, F., & Whitelaw, J. H. (1978). Asymmetric flows and instabilities in symmetric ducts with sudden expansions. Journal of Fluid Mechanics, 84(1), 13-31.

Choi, H.H., and Nguyen, J. (2016). Numerical investigation of backward facing step flow over various step angles. *Procedia Engineering*, 154, 420-425.

Dange, A. (2010). Modeling of turbulent particulate flow in the recirculation zone downstream of a backward facing step preceding a porous medium. *MS Thesis*. Oklahoma State University.

Darmawan, S., and Tanujaya, H. (2019). CFD Investigation of Flow Over a Backward-facing Step using an RNG k-ε Turbulence Model. *Mechanical Engineering*, 10(2).

Erturk, E. (2008). Numerical solutions of 2-D steady incompressible flow over a backward-facing step, Part I: High Reynolds number solutions. *Computers and Fluids*, 37(6), 633-655.

Gautier, N., and Aider, J.L. (2014). Feed-forward control of a perturbed backward-facing step flow. *Journal of Fluid Mechanics*, 759, 181-196.

Gualtieri, C. (2005). Numerical simulations of laminar backward-facing step flow with FemLab 3.1. *ASME Fluids Engineering Division Summer Meeting and Exhibition*, Houston, TX, USA.

Jongebloed, L. (2008). Numerical study using FLUENT of the separation and reattachment points for backwards-facing step flow. *MS thesis.* Rensselaer Polytechnic Institute.

Jehad, D.G., Hashim, G.A., Zarzoor, A.K., and Azwadi, C.N. (2015). Numerical study of turbulent flow over backward-facing step with different turbulence models. *Journal of Advanced Research Design*, 4(1), 20-27.

Jovic, S., and Driver, D.M. (1994). Backward-facing step measurements at low Reynolds number, Reh= 5000. *NASA technical memorandum*, 108807, 94035-1000.

Kopera, M.A., Kerr, R.M., Blackburn, H., and Barkley, D. (2017). Simulation of turbulent flow over a backward-facing step at Re= 9000. *Physics of Fluids*. in review.

Krishnamoorthy, C. (2007). Numerical analysis of backward-facing step flow preceding a porous medium using FLUENT. *MS Thesis*. Oklahoma State University.

Kumar, A., and Dhiman, A. K. (2012). Effect of a circular cylinder on separated forced convection at a backward-facing step. *International Journal of Thermal Sciences*, 52, 176-185.

Lee, T., and Mateescu, D. (1998). Experimental and numerical investigation of 2-D backward-facing step flow. *Journal of Fluids and Structures*, 12(6), 703-716.

Louda, P., Příhoda, J., Kozel, K., and Sváček, P. (2013). Numerical simulation of flows over 2D and 3D backward-facing inclined steps. *International Journal of Heat and Fluid Flow*, 43, 268-276.

Moosavi, R., Moltafet, R., Lin, C.X., and Chuang, P.Y.A. (2021). Numerical modeling of fractional viscoelastic non-Newtonian fluids over a backward facing step–Buoyancy driven flow and heat transfer. Thermal Science and Engineering Progress, 21, 100767.

Park, H.S., and Thornber, B. (2018). DES of Flow Past an Oscillating Cylinder Located Downstream of Backward-Facing Step. *21st Australasian Fluid Mechanics Conference*. Perth, Australia.

Prihoda, J., Zubik, P., Sulc, J., and Sedlar, M. (2012). Experimental and numerical modelling of turbulent flow over an inclined backward-facing step in an open channel. *Communications-Scientific letters of the University of Zilina*, 14(4A), 6-12.

Ratha, D., and Sarkar, A. (2015). Analysis of flow over backward facing step with transition. *Frontiers of Structural and Civil Engineering*, 9(1), 71-81.

Selimefendigil, F., and Öztop, H.F. (2013). Identification of forced convection in pulsating flow at a backward facing step with a stationary cylinder subjected to nanofluid. *International Communications in Heat and Mass Transfer*, 45, 111-121.

Selimefendigil, F., and Öztop, H.F. (2015). Numerical investigation and reduced order model of mixed convection at a backward facing step with a rotating cylinder subjected to nanofluid. *Computers and Fluids*, 109, 27-37.

Sparrow, E. M., & Kalejs, J. P. (1977). Local convective transfer coefficients in a channel downstream of a partially constricted inlet. International Journal of Heat and Mass Transfer, 20(11), 1241-1249.

Tihon, J., Pěnkavová, V., and Pantzali, M. (2010). The effect of inlet pulsations on the backward-facing step flow. *European Journal of Mechanics-B/Fluids*, 29(3), 224-235.

Tihon, J., Pěnkavová, V., Havlica, J., and Šimčík, M. (2012). The transitional backward-facing step flow in a water channel with variable expansion geometry. *Experimental Thermal and Fluid Science*, 40, 112-125.

Togun, H., Abdulrazzaq, T., Kazi, S.N., Badarudin, A., Ariffin, M.K.A., and Zubir, M.N.M. (2014). Numerical study of heat transfer and laminar flow over a backward facing step with and without obstacle. *International Journal of Mechanical, Aerospace, Industrial and Mechatronics Engineering*, 8(2), 2.

Uruba, V., Jonáš, P., and Mazur, O. (2007). Control of a channel-flow behind a backward-facing step by suction/blowing. *International Journal of Heat and Fluid Flow*, 28(4), 665-672.

Wang, F.F., Wu, S.Q., and Zhu, S.L. (2019). Numerical simulation of flow separation over a backward-facing step with high Reynolds number. *Water Science and Engineering*, 12(2), 145-154.

Yao, S. (2000). Two dimensional backward facing single step flow preceding an automotive air-filter. *Ph.D. Thesis.* Oklahoma State University